

Technical Note

Flood Distance Algorithms and Fault Hidden Danger Recognition for Transmission Line Towers Based on SAR Images

Lianguang Liu ^{1,2}, Rujun Du ^{1,*}  and Wenlin Liu ²

¹ State Key Laboratory of Alternate Electrical Power System with Renewable Energy Sources, North China Electric Power University, Beijing 102206, China

² Dezhou Tianhe Benan Electric Power Technology Co., Ltd., Dezhou 253000, China

* Correspondence: 1172201051@ncepu.edu.cn; Tel.: +86-18911800856

Received: 8 June 2019; Accepted: 8 July 2019; Published: 10 July 2019



Abstract: Synthetic Aperture Radar (SAR) has been extensively used in the monitoring of natural hazards such as floods and landslides. Predicting whether natural hazards will cause serious harm to important facilities on the ground is an important subject of study. In this study, the distance between the water body and the tower and the flood ratio in the search area and the elevation are defined as the evaluation indicators of the flood hazard of the tower, indicating whether flooding will threaten the safety of the transmission line tower. Herein, transmission tower flood identification algorithms based on the center distance of the tower and the grid distance of the tower are proposed. SAR satellite image data of the flood with a resolution of 10 m are selected to prove the feasibility and effectiveness of the proposed fault identification algorithm. The simulation results show that the SAR satellite image data with a resolution of 10 m can identify the distance accuracy of the transmission tower flood hazard by up to 7 m, which can be used to identify the flood fault of the transmission line tower.

Keywords: hazard prevention; flood hazard; hidden danger identification; tower failure

1. Introduction

As the scale of the power grid increases, the scope, and thus the workload, of power grid inspections continue to expand. At present, power inspections in most countries still rely on the manual recording of data, which has disadvantages such as high cost, dangerous working conditions, and absence of inspection. Over the past two decades, aerial inspections have been employed [1], which can greatly improve detection efficiency and precision. However, this method is restricted by factors such as flight safety, airline control, weathers changes, and refueling. Unmanned aerial vehicles (UAV) are not widely used because of the safety issues and a lack of durability [2–4]. For these reasons, the development of satellite technology provides a new and important means of fault detection and hazard prediction for transmission lines.

Floods account for 40% of the losses caused by natural hazards worldwide. Flood hazards cause damage to the power grid by submerging power equipment and thus causing short circuit damage, internal discharge damage, and moisture damaged. Furthermore, the foundation of the transmission line tower can be washed away by floods, which may cause the tower to collapse, thus causing power interruptions and threatening the safe and stable operation of the power system [5–8]. In recent years, the once-in-a-century floods in the Oder River and Nice River basins flowing through Poland, Czech Republic, Austria, and Germany caused economic losses of 5.9 billion dollars. Two catastrophic floods in the central and northern United States caused economic losses of 2215 billion dollars. In China,

Jiangxi and Hebei suffered severe floods due to heavy rainfall, many substations and several lines were shut down, and more than 300,000 users suffered blackouts [9,10]. In June 2015, in Georgia, floods damaged Tbilisi's transmission lines, resulting in power outages for about 22,000 consumers in two districts of Tbilisi. In the summer of 2016, continuous heavy rainfall in the Hubei Province of China caused severe floods in Tianmen, resulting in the outage of several substations, resulting in a total of 30·10 kV line failures, involving 1158 stations and 115,276 users. In the Fujian Province of China, floods and geological hazards occurred an average of 3.3 times a year over the past 10 years, resulting in an average annual direct economic loss of 3.6 billion yuan [11–13]. If transmission line flood faults can be located quickly, the loss can be reduced. Therefore, an identification algorithm of transmission line tower flood faults is a subject that needs to be studied.

Synthetic Aperture Radar (SAR) has been widely used in hazard monitoring. This paper proposes the use of SAR images to identify flood faults on transmission lines. At present, on the basis of the SAR image water feature, the water body part of an image can be accurately extracted [14]; this can be done in different scenarios such as floods in forest areas or floods in cities [15,16]. The introduction of some improved algorithms also makes the extraction range of floods more accurate [17–32]. In [33,34], methods for searching for mountain fire faults of transmission line towers are proposed. By combining our research with the abovementioned methods, we propose an identification algorithm for flood faults in transmission line towers. This is of great significance for the operation and maintenance of transmission towers.

The objectives and novelty of the study are as follows:

(1) This is the first study based on SAR satellite imagery on hidden flood hazards related to transmission line towers. When hazards occur, SAR has the advantages of a quick response, accurate positioning, and a wide coverage, all of which help identify towers that may be infringed upon by floods and aid inspectors design targeted emergency repair schemes to minimize the economic losses caused by power outages;

(2) We propose two fast methods to calculate the shortest distance between tower and flood based on the center distance of the tower and the grid distance of the tower. Furthermore, we can find the nearest flood within a certain distance between tower and tower. The two algorithms fill in the methodological gaps of calculating the shortest distance from tower to flood;

(3) We propose that the shortest distance from tower to flood, the proportion of flood in a search area and the elevation difference between the tower base and the flood level should be taken as indicators to give a certain weight to evaluate the hazard degree of the tower. This evaluation method is a rapid evaluation made in emergency situations when floods occur. It can reflect the distribution of floods around towers and the hazard degree of towers.

2. Flood Recognition Algorithm Based on SAR Imaging

2.1. Image Preprocessing

The SAR radar echo signals are superimposed onto each other, which causes the radar image to produce granular spots. This phenomenon is the result of the influence of speckle noise, which is the main cause of SAR image noise. The existence of speckles has an impact on the interpretation and extraction of objects in the image, especially in terms of the extraction and recognition of the contours and edges of the target, and may even cause the disappearance of features. In order to extract and identify the feature information more accurately, it is necessary to weaken the fluctuation of the luminance value and the influence of the speckle noise through filtering.

A comparison of the filtering effects of various filtering methods [30] on SAR images shows Lee filtering to be an effective option.

2.2. Identification Model For Flood Areas

For the processing of SAR images, threshold segmentation can be used to extract water bodies. This principle is based on the low scatter value of the water body in the SAR image. It is achieved by setting a suitable threshold to mark the image; thus, the values less than the threshold portion become the water body, and the portions larger than the threshold portion become the background, forming a binary image. The advantage of this algorithm is that it is fast and the principle is simple; however, the determination of the threshold is difficult. Among several commonly used threshold segmentation methods, Otsu's optimal global threshold segmentation method has a low false alarm rate and high water extraction accuracy [31]. The algorithm is as follows:

An image histogram distribution can be expressed by

$$P_q = \frac{n_q}{n} \quad q = 0, 1, 2, \dots, L-1, \quad (1)$$

where n is the total number of image pixels, n_q is the number of pixels with a grayscale of q , and L is the number of all possible gray levels in the image. Suppose the target area C_1 contains gray levels $[0, 1, 2, \dots, k]$, C_2 contains gray levels $[k+1, \dots, L-1]$, and the threshold is k , the largest inter-class variance $\sigma_B^2(k)$ is

$$\sigma_B^2(k) = P_1(k)[m_1(k) - m_G]^2 + P_2(k)[m_2(k) - m_G]^2 \quad (2)$$

$P_1(k)$ and $P_2(k)$ are the percentage of pixels of C_1 and C_2 in the whole image, respectively, $m_1(k)$ and $m_2(k)$ are the average gray value of the pixels in the C_1 and C_2 regions, respectively, and m_G is the average gray value of the whole image. The average gray value of the gray level k can be obtained by the following formula:

$$m(k) = \sum_{i=0}^k ip_i. \quad (3)$$

Expand Equation (2) and substitute $P_2(k) = 1 - P_1(k)$ to get the following formula:

$$\sigma_B^2(k) = \frac{[m_G P_1(k) - m(k)]^2}{P_1(k)[1 - P_1(k)]}. \quad (4)$$

Determining the values of m and $P_1(k)$ can determine the between-class variance. Under the condition of maximum between-class variance, the threshold of the segmented image is easier to determine. Since k is an integer in the range $[0, \dots, L-1]$, it is possible to find the k value at the maximum of the variance between classes by continuous loop calculation, where k is the optimal threshold. When the k value is not unique, the average of the plurality of k values is the optimal threshold. The ratio of between-class variance to the grayscale variance of the total image is a separability measure that divides the image into two categories:

$$\eta(k) = \frac{\sigma_B^2(k)}{\sigma_G^2(k)}. \quad (5)$$

The algorithm automatically calculates the segmentation threshold by finding the maximum between-class variance between the two types of features. Therefore, there is a good segmentation effect when there is a significant difference between the gray value of the object in the region of interest and the gray value of other features. That is to say, the gray value frequency distribution of the image has obvious "peak and valley" characteristics, and the larger the difference between the peak value and the valley value, the more obvious the segmentation effect.

The grayscale value at the original image point (x, y) is $I(x, y)$, and the target in the original image is extracted with the threshold k . Herein, a is the value of the background and b is the value of the target. The binary image $F(x, y)$ is generated as follows:

$$F(x, y) = \begin{cases} a, & I(x, y) \geq k \\ b, & I(x, y) < k. \end{cases} \quad (6)$$

The value of a is 1, and the value of b is 0. The original image completes the binary transformation to extract the water body.

2.3. Flood Failure Evaluation Index

The severity of flood damage to the tower is positively related to the distance and the elevation. The possibility of tower collapse caused by flood scouring near the water area is far greater than that caused by a flood far away from the water area. The elevation difference between the tower base and the flood level can reflect whether the tower is submerged. The distance and the elevation can be used as the main parameter for the evaluation of hidden dangers of flood failure. On the basis of the SAR image taken by satellite, the flood area is extracted through image processing. Combining this with the information of the transmission line tower account, a judgment on whether the tower has been flooded is made, and the hazard situation of the transmission line is preliminarily evaluated. If the tower is not flooded, the distance between the tower and the edge of the flood should then be determined to quickly judge the impact of the flood hazard on the transmission line.

An image is made up of pixels, and each point in the image can be converted into coordinates. According to the account information of the tower, visual interpretation, and coordinate picking, the pixel coordinate point set of the tower in the binary image extracted by the water body is determined as follows:

$$U = \{a_1(x_1, y_1), a_2(x_2, y_2), \dots, a_n(x_n, y_n)\} \quad (7)$$

where U is the set of tower coordinates, a_i is the name of the tower, x_i is the abscissa of the pixel coordinates of the binary image, and y_i is the ordinate of the pixel coordinates of the binary image. $F(x_i, y_i)$ is the value of the point (x_i, y_i) in the binary image. If $F(x_i, y_i) = 0$, it shows that the tower is located in the water extraction part, the tower has been flooded, and the tower is most seriously affected. If $F(x_i, y_i) = 1$, the tower is located in the non-water part and so has not been flooded. However, there may still be potential flood hazards. The elevation layer and the distance between the tower and water body boundary should be calculated. A search for transmission line towers around the waters that may be endangered by floods should be conducted to determine the extent of the damage to the towers. The elevation model can be extracted from any public available elevation model such as SRTM or ASTER Global Digital Elevation Model. The elevation model is established to calculate the elevation difference between the flood level and the tower foundation. The specific content of the algorithm will not be discussed in this paper. The calculation of the distance between the towers and the water body boundary is described below.

3. Tower Flood Failure Distance Algorithm and Criterion

On the basis of the extracted water body binary image characteristics, a search algorithm for the center distance of the tower and a search algorithm for the tower base grid distance are proposed.

3.1. Tower Center Distance Search Algorithm

According to operating experience and flood control standards, floods beyond 3 km do not pose a threat to transmission lines. Therefore, it is only necessary to search for transmission line towers within 3 km of the water body. In addition, the safe distance can be increased or decreased as needed. A circular area of 3 km around the tower is used as the search area. If there is a water body in the

search area, it can be judged that there is a flood hazard on the transmission line. On the basis of the SAR image and the tower information, the position information of the tower that may be affected and the latitude and longitude information of each point of the image are determined.

In Figure 1, we choose the image coordinates. The upper left corner is the coordinate origin, the horizontal axis is the x-axis, and the vertical axis is the y-axis. The two towers A_1 and A_2 have a circle with a radius of R ($R = 3\text{km}$) centered on A_1 and A_2 . L_1 and L_2 are water body boundaries, and between L_1 and L_2 are water bodies. Let the image resolution be M (m), and each pixel is an $M \times M$ rectangle. From this it can be obtained that $M \times r = 3000$, r is the radius in the image, and the unit is a pixel. The equation for indicating the boundary circle of the A_1 tower search area by coordinates is

$$(x - x_1)^2 + (y - y_1)^2 = \left(\frac{3000}{M}\right)^2. \quad (8)$$

Points in the search area satisfy the following formula:

$$(x - x_1)^2 + (y - y_1)^2 < \left(\frac{3000}{M}\right)^2. \quad (9)$$

The search can be conducted from the center to the outside. If the existence point (x_i, y_i) satisfies Equation (9) and $F(x_i, y_i) = 0$, then there is a water body in the search area of the tower. The nearest distance from the water body to the tower should then be calculated. The distance between the tower $A_1(x_1, y_1)$ and the water body is calculated according to the distance formula between two points:

$$d = \sqrt{(x_1 - x_i)^2 + (y_1 - y_i)^2}. \quad (10)$$

The calculation accuracy is $\sqrt{2}M/2$.

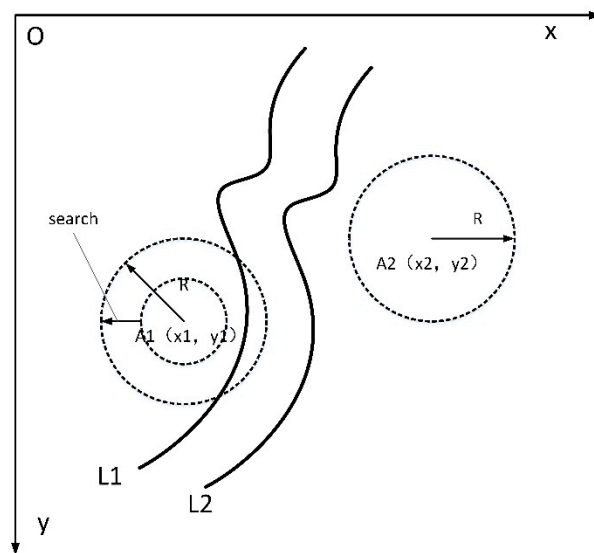


Figure 1. Tower center distance search method.

3.2. Tower Base Grid Distance Search Algorithm

The tower center distance search method can judge the tower flood failure. However, when the search area is wide and the number of towers is large, the calculation cost is high and so it takes a long time. The circular search area can be changed to the grid search area of the tower base. With the tower as the center, a square grid search area with a side length of 6 km is made. The four vertices of the grid search area are A, B, C, and D, as shown in Figure 2.

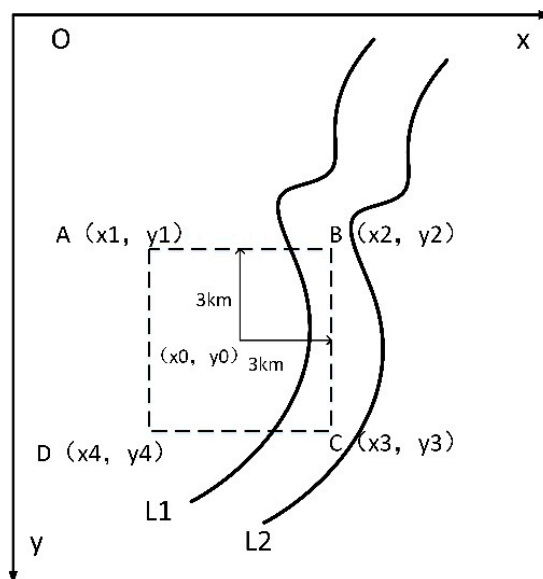


Figure 2. Tower base grid distance search method.

The coordinates of the tower are (x_0, y_0) ; the coordinates of the four endpoints are $A(x_1, y_1)$, $B(x_2, y_2)$, $C(x_3, y_3)$, and $D(x_4, y_4)$. The mathematical relationship between x_2 and x_0 is

$$M \cdot (x_2 - x_0) = 3000. \tag{11}$$

This is formulated as

$$x_2 = \frac{3000}{M} + x_0. \tag{12}$$

By the same logic,

$$\begin{cases} x_1 = x_4 = x_0 - \frac{3000}{M} \\ x_2 = x_3 = x_0 + \frac{3000}{M} \\ y_1 = y_2 = y_0 - \frac{3000}{M} \\ y_3 = y_4 = y_0 + \frac{3000}{M} \end{cases}. \tag{13}$$

It can be concluded that the points in the search area satisfy Equation (14). If there are points (x_i, y_i) in the binary image, which make $F(x_i, y_i) = 0$ and satisfy (14), then there is a potential flood hazard in the towers search area. According to Equation (10), the minimum distance between the tower and water body is calculated.

$$\begin{cases} x_0 - \frac{3000}{M} \leq x_i \leq x_0 + \frac{3000}{M} \\ y_0 - \frac{3000}{M} \leq y_i \leq y_0 + \frac{3000}{M} \end{cases} \tag{14}$$

Compared with the tower center distance search method, the tower base grid distance search method does not need to calculate the distance for each point, and the search process only involves a coordinate value comparison, which can improve the calculation speed of the algorithm. However, the grid search method searches for a square grid and searching near the vertex (a distance greater than 3 km) can cause false alarms. This type of false alarm can be avoided by distance quantitative comparison.

3.3. Flood Failure Criterion Based on Distance Algorithm, Flood Ratio and the Elevation

In the binary image, the function value of the water body is 0, and the function value of the non-aqueous body is 1. \bar{F} , the average value of the function in the search area, equals

$$\bar{F} = \frac{1}{n} \sum_{i=0}^n F(x_i, y_i). \tag{15}$$

If $\bar{F} = 1$, there is no water body in the search area, and there is no potential flood hazard for the transmission tower. If $\bar{F} < 1$, there are water bodies in the search area, and there are potential flood hazards for transmission line towers. The easiest way to get the F number is to count the number of ones within the window of 3000×3000 m and divide it by the number of pixels.

H is the flood ratio. The flood ratio can reflect the extent of flooding in the search area. The larger the H , the wider the flood range in the search area, and the greater the likelihood and severity of the flood damage to the tower.

The elevation Δh can reflect the difference in height between the tower base and the flood level. The smaller the Δh is, the closer the height of tower foundation and flood level is, and the greater the threat of flood disaster to tower is.

On the basis of the standard for construction, operation of the transmission line towers and overhaul experience accumulated over the years and the flood control standard, the flood hazard coefficient V of the tower is designed to measure the hazard situation. The coefficient V is mainly determined by the distance d between the tower and the flood, the flood ratio H in the search range of the tower and the elevation Δh as shown in the following equation:

$$V = C_1 \frac{d}{3000} + C_2(1 - H) + C_3 \frac{\Delta h}{1000} \quad (16)$$

The distance d from the tower to the flood is divided by the search radius (3 km), reflecting the distance between the flood in the search range and the tower. The closer the distance, the smaller the value, and the greater the degree of danger; C_1 is the weight of the distance. H is the proportion of floods. The larger the flood ratio, the larger the number. When the value is adjusted to $1 - H$, the larger the H , the smaller the value, and the weight coefficient is C_2 . The elevation Δh between the tower base and the flood level is divided by 1000. If $\Delta h > 1000$ m, we think the tower is absolutely safe according to "Flood Control Standard of Transmission Line (GB50201-2014)". If $\Delta h < 1000$ m, the smaller $\Delta h/1000$ (a value less than 1) is, the closer the elevation difference between the tower base and flood level, the smaller the value, and the greater the degree of danger. C_3 is the weight of the elevation. Therefore, the closer the flood, the larger the flood ratio in the search area, the closer the elevation between the tower base and flood level, the smaller $d/3000$, $1 - H$ and $\Delta h/1000$ will be, and the smaller the V , the greater the degree of danger. In Formula (16), $C_1 = 0.3C_2 = 0.2C_3 = 0.5$. V is a number less than 1. The smaller the V , the greater the threat of flood to towers. By calculating the distance d and the flood ratio H and the elevation Δh in the search range of the tower, the tower flood hazard coefficient V is calculated. Thereafter, it is possible to judge the severity of the flood. On the basis of the statistical data of the State Grid, the Southern Power Grid and the Meteorological Bureau, the V coefficients of transmission lines and towers in some flood-stricken areas in China are calculated. According to the severity of actual hazards and the potential hazards of poles and towers, the hazard classification is divided according to the calculation of the coefficient and the actual situation. The damage degree of the tower is divided as follows:

1. When $d = 0$ m, the tower has been flooded and it is judged to be a super hazard;
2. When $V < 0.1$, the degree of hazard is judged to be in the A level;
3. When $0.1 \leq V < 0.4$, the degree of hazard is judged to be in the B level;
4. When $0.4 \leq V < 1$, the degree of hazard is judged to be in the C level.

After the hazard level is judged, it should be released quickly so that it can be utilized in time. The warning information released includes tower location, line name, voltage level, flood impact area, the location of flood relative to the tower, the distance between flood and tower, the elevation between the tower base and the flood level, etc. This is all possible as a result of the advantages of rapid satellite inspection and accurate positioning. According to the terrain, the soil, and the season, the values of C_1 , C_2 and C_3 can be changed appropriately to adjust classification of the damage level caused by floods. According to various sets of data (the "Standard for flood control GB50201-2014" and "Research

on hazard damage characteristics and hazard prevention technology of distribution network flood geological hazards”, the “Application of Correction Technique of Initial Soil Water Storage Capacity Correction in Flood Forecasting”, and the “Study on the Supply And Demand of Soil Erosion Control Service and Flood Control Service in Linfen Section of Fenhe River Basin”), the proportion of C_1 can be appropriately increased when the climate is humid and the soil is loose. This is because even if there is a certain distance from the flood, continuous erosion by the flood may cause the tower foundation to collapse, leading to tower collapse.

4. Case Analysis

To perform the analysis, the backscattering SAR image satellite image (resolution 10 m) in the flood-prone area is selected and Lee filter processing performed. After the processing, the water body is extracted using the threshold segmentation method, as shown in Figures 3–5.

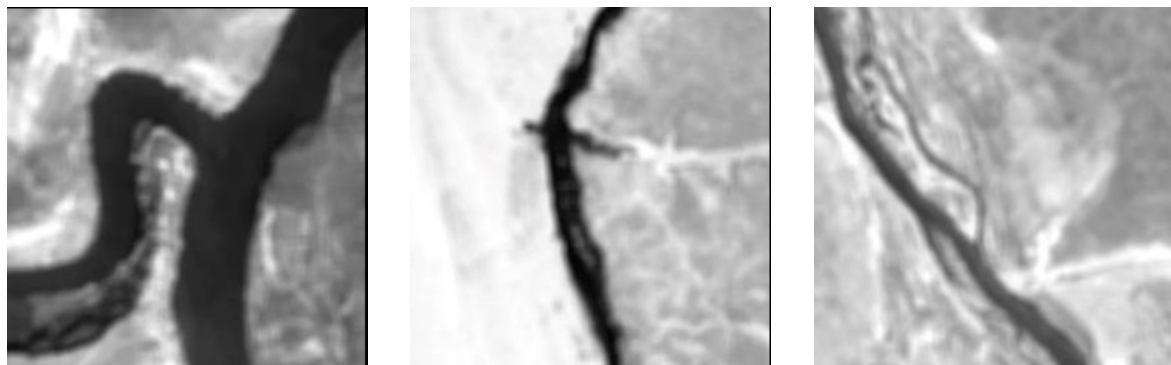


(a) Example 1

(b) Example 2

(c) Example 3

Figure 3. The original images.



(a) Example 1

(b) Example 2

(c) Example 3

Figure 4. Images after Lee filtering.

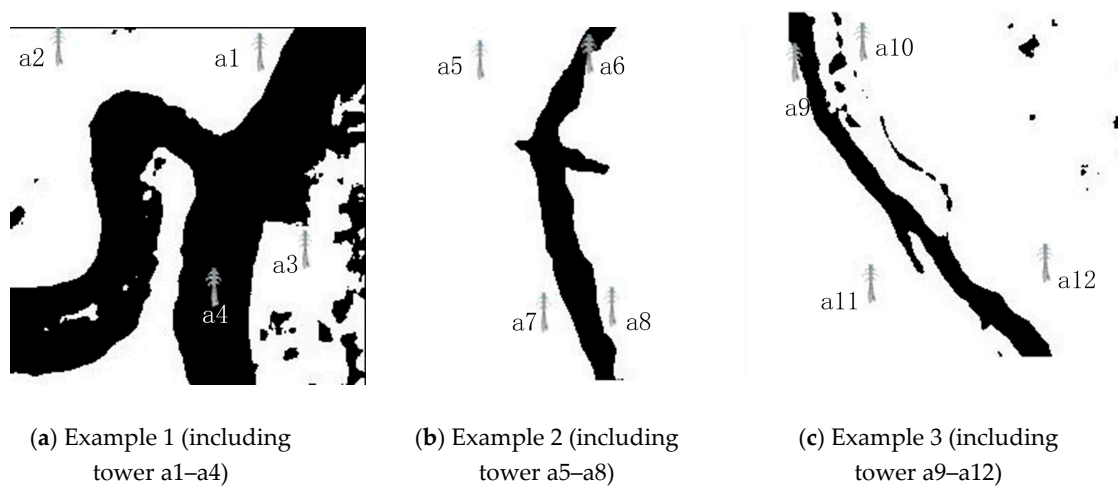


Figure 5. The binary images of the water body after threshold segmentation.

A set of points was randomly selected around the water bodies of the three binary images of Figure 5, and each map selected four points, which are a_1, a_2, \dots, a_{12} , as the positions of the towers. We calculated the distance from flood to tower, the elevation difference between flood level and tower foundation, and the flood ratio within the search range. The flood hazard coefficient was calculated. The results are shown in Table 1.

Comparing the calculation time of the two algorithms in Table 1, the tower grid distance algorithm is faster than the tower center distance algorithm. In order to make the test results more general, we randomly picked points in the flood area of Figure 3 as the tower coordinates. This was done to verify that the algorithm can accurately calculate the flood distance and make hidden danger evaluations no matter where the tower was located. Tower a4 was located in the water body, which was used to simulate the actual situation when a tower is submerged by flooding. The danger level S also reflects the fact that the tower was submerged by the flood, which proves the reliability of the calculation results. The results show that the combination of the distance and the elevation can accurately reflect the hidden flood hazards of transmission line towers. At the same time, the elevation reduces commission errors. The image resolution of the example is 10 m, and the calculation distance accuracy reaches 7 m. When using higher resolution images, the accuracy increases. In addition, combined with the water body around the tower, the hidden danger coefficient can effectively reflect the severity of the flood hazard caused by the tower.

Table 1. Simulation results.

Tower Number	Tower Coordinates	Coordinates of the Nearest Flood	The Alarm Distance (m)	Flood Ratio (%)	The Elevation Δh (m)	V Coefficient	Calculation Time of the Tower Center Distance Algorithm(s)	Calculation Time of Tower Base Grid Distance Algorithm(s)	The Affected Level
a1	(178,15)	(189,16)	110.45	11.4	350	0.2088	0.0212	0.0198	B
a2	(33,20)	(71,3)	416.29	10.5	240	0.1826	0.0288	0.0263	B
a3	(203,154)	(204,137)	170.29	12.3	270	0.1766	0.0224	0.0211	B
a4	(145,186)	(145,186)	0	45.5	0	0.0910	0.0162	0.0150	S
a5	(57,32)	(103,46)	480.83	3.8	110	0.1107	0.0299	0.0292	B
a6	(137,32)	(127,29)	104.40	20.1	170	0.1356	0.0188	0.0180	B
a7	(106,219)	(119,213)	143.17	14.4	130	0.1081	0.0231	0.0220	B
a8	(153,222)	(146,225)	76.16	22.5	200	0.1526	0.0185	0.0177	B
a9	(6,53)	(15,49)	98.49	30.1	80	0.1100	0.0171	0.0165	B
a10	(58,37)	(52,45)	100	18.7	50	0.0724	0.0191	0.0182	A
a11	(62,212)	(97,189)	418.80	4.1	160	0.1301	0.0330	0.0310	B
a12	(194,196)	(178,226)	340	8.3	130	0.1156	0.0263	0.0242	B

5. Discussion

The calculated results show that the accuracy of the two distance algorithms is the same. Because the two algorithms search for the water points around the towers comprehensively, and find the shortest distance from towers, the location of the water points is the same, but the search methods are different, resulting in different calculation speeds. In terms of algorithm speed, the tower-based grid search algorithm is faster. The reason for this is that compared with the tower center distance search method, the tower base grid distance search method does not need to calculate the distance of each point, and only involves the comparison of coordinate values in the search process, which shortens the calculation time. However, the search area divided by the grid search method is a square grid, and the water near the vertex (a distance greater than 3 km) may cause a false alarm. This kind of false alarm can be avoided by comparing the calculated distance with the safe distance quantitatively.

By comparing Figure 5a with Figure 3a, the non-water part is extracted from the binary image. The accuracy of the binary image extracted by water threshold segmentation has a certain influence on the calculation results of the shortest distance between tower and water body [33]. If the non-water part is extracted from the binary image, the water point calculated to be the shortest distance between the tower and the water point may be the extracted non-water point, resulting in errors in distance calculation and even false alarms [35,36]. If the actual water body is not extracted, the shortest distance calculated may not be the actual shortest distance (with other water body points being closer to the tower). At the same time, the calculation results of flood proportion in the tower search area also produce some errors. In order to make the evaluation index of flood hidden danger scenario and the calculation of the shortest flood distance more accurate, it is necessary to improve the accuracy of extracting binary maps from flood areas. In addition to the traditional Lee filtering and Otsu threshold segmentation, an improved method for water extraction is proposed in the literature [37–43]. In [25], the selection criterion of target blocks with water is proposed. Gauss distribution is used to fit the backscattering coefficient of ground objects. Combined with the improved Gamma model, the optimal threshold position is determined, the optimization criterion is constructed, the target threshold is solved by adaptive iteration, and the threshold accuracy is increased. In [37], the identified seed point is confirmed locally based on two parameters corresponding to intensities and percentage of occurrence of intensities around the seed. A densely populated range around the seed point is computed. From the seed point, regions are grown until the intensity value of that point is within the range to complete the task, with all flooded regions captured in the SAR image. Reference [38] proposes the Bayesian network, a system whereby remote sensing data (such as multi-temporal SAR intensity image and interferometric SAR coherent data) are combined with geomorphology and other ground information to coordinate the use of different information layers, which helps to more accurately detect flood-affected areas, and reduce false positives and omissions. Reference [39] proposes the use of interferometric data to distinguish zones where water receded from areas where it persisted for a longer time, and in one case, to measure changes in water level. In [40], water categories from Landsat images are extracted and water categories from TerraSAR-X images are subtracted; the remaining water represents the flooded area. According to the different scenarios of transmission line corridors, different threshold segmentation methods can be selected to achieve the optimal extraction of the water body.

According to the environment of transmission lines, considering the local temperature, humidity, soil, plants and other factors, the C_1 , C_2 and C_3 values of flood hidden danger coefficient calculation formula are adjusted based on the analytic hierarchy process; in this way, the flood hidden danger coefficient can be widely and rationally used to evaluate the flood hidden danger of poles and towers, and whether poles and towers are threatened by floods can be reasonably judged [44–46]. At the same time, the safe distance from the tower to the flood can also be adjusted according to the environmental conditions of the transmission lines. For example, in areas with loose soil, the foundation of transmission line poles and towers may be affected to a certain extent even at greater distances from the flood, and so the impact of the flood is larger. How to set the most reasonable safe distance and the value of

C_1 , C_2 and C_3 according to the specific environment and the service life of the tower, considering the influence of various factors comprehensively, is a problem worthy of further study [47–51].

The purpose of this study was to create a system in which the towers which suffered from flood hazards and transmission line towers that may have potential hazards are discovered quickly, to make a preliminary evaluation of the hazard situation, to provide a reference and basis for the emergency repair of transmission line towers, and to reduce the economic losses caused by power blackouts in flood hazard scenarios. This paper is a preliminary judgment of tower flood hazard scenarios based on SAR images in which only a limited number of indicators are selected; therefore, the most intuitive distance and the elevation in the satellite image is chosen as the main measure factor. If the tower is submerged, the design scheme should focus on dealing with it. If it is not submerged, it should be properly dealt with according to the distance, the elevation and the actual environment. The elevation is the determining factor signifying whether a tower is submerged. The distance can reflect whether there is a hidden danger. When the position of the tower is higher than the horizontal plane, the tower is not submerged, but it cannot be guaranteed that the tower is absolutely safe. With the erosion from water, the foundation soil of the tower may be loose, which may cause hidden dangers for the tower. Therefore, the distance cannot be ignored, and the closer the distance is, the more likelihood there is a potential problem. On the other hand, the transmission power could be located on the slope of a small hill 30 meters above the flood and less than 1 km from the flood front edge and there is no danger for the tower. The elevation will help the system to reduce false alarms. Equation (16), which is related to hazard discrimination, shows that the closer the distance and the smaller the elevation difference, the greater the hidden danger. The combination of distance and elevation makes the result more accurate and comprehensive. At the same time, the proportion of floods in the search area helps to assist in judging the hazard situation and potential flood hazards of each tower. Combined with the results of the example, we think that the proposed index and evaluation method can be used to judge the hidden danger degree of tower flooding.

In addition, the velocity and duration of the flood are also influencing factors. However, they are not easy to visualize in satellite imagery. Flood velocity, duration, water level, and other factors do affect the tower, but it is impossible to consider all factors as indicators because of the limitations of the length of the article.

This is the first study into transmission line tower faults based on satellite images. Our system involves choosing the SAR images to study the impact of flood hazards on transmission line towers, selecting the distance and the elevation index, maximizing the use of limited information, responding quickly when a hazard occurs, and providing sufficient references and guidance for line inspections. In summary, the authors believe that the choice of distance and the elevation as the main indicator is a suitable choice at this stage. In future studies, we will try to consider as many indicators as possible, including distance, water level, velocity, soil, humidity and so on, to make the tower flood risk assessment more accurate.

A future research direction may be the establishment of a high-resolution satellite image database of the transmission line corridor. Through the comparison of multi-stage satellite images, various kinds of geological hazards are found, and the use of higher resolution satellite images is conducive to improving the accuracy of the calculations. An intelligent algorithm is used to identify the location of the pole and tower, which makes the whole process more automated. By identifying and analyzing the environment of the line, the appropriate threshold segmentation algorithm can be selected intelligently.

6. Conclusions

On the basis of backscattering water SAR imaging, this paper proposes two kinds of tower flood failure algorithms. By combining these with the distance factor, the flood ratio and the elevation, the hidden danger coefficient can be calculated, which can effectively judge the flood failure of the transmission tower.

Through testing, the tower center distance algorithm and the grid distance algorithm can accurately calculate the nearest distance between the tower and flood. A 10 m resolution image can reach an accuracy of 7 m, with the grid distance algorithm being the faster of the two.

The binary images obtained using threshold segmentation influence the judgment. Extracting the non-water body part causes the flood hazard to be falsely reported. The water body information can be extracted by combining various threshold segmentation methods to improve the accuracy.

In future research, the tower coordinates can be intelligently identified without the need for manual selection. When searching the same area again, the tower position is determined directly according to the latitude and longitude coordinates, and the database is perfected to construct an expert system.

Author Contributions: Conceptualization, L.L.; Data curation, W.L.; Formal analysis, R.D.; Methodology, L.L.; Resources, W.L.; Supervision, L.L.; Validation, R.D.; Writing—original draft, R.D.; Writing—review and editing, R.D. and L.L.

Funding: This research received no external funding.

Acknowledgments: The authors would like to express gratitude to Junwei Han, who provided much help and instruction in data processing.

Conflicts of Interest: The authors declare no conflict of interest.

References

1. Yu, D.; Wu, Y.; Chen, F. Application of helicopter patrol technology in UHV AC transmission line. *Power Syst. Technol.* **2010**, *34*, 29–32.
2. Peng, X.; Liu, Z.; Mai, X.; Luo, Z.; Wang, K.; Xie, X. A transmission line inspection system based on remote sensing: System and Its Key Technologies. *Remote Sens. Inf.* **2015**, *30*, 51–57.
3. He, R.; Lu, C.; Yu, X.; Liu, X.; Zhang, X.; Mu, X.; Feng, G.; Wang, Y.; Wu, K. Development of a new type of unmanned transmission line inspection airship. In Proceedings of the International Conference on Measuring Technology & Mechatronics Automation IEEE Computer Society, Changsha, China, 10–11 February 2018; pp. 118–120.
4. Li, J.; Wang, L.; Shen, X. Unmanned aerial vehicle intelligent patrol-inspection system applied to transmission grid. In Proceedings of the 2018 2nd IEEE Conference on Energy Internet and Energy System Integration, Beijing, China, 20–22 October 2018; pp. 1–5.
5. Wang, Z. *The Comprehensive Assessment of the Power Loss and the Economic Impact of the Power Outages under the Flooding*; Hunan University: Changsha, China, 2012.
6. Banks, D.R. Telecomm disaster recovery planning for electric utilities. In Proceedings of the 2005 Rural Electric Power Conference, San Antonio, TX, USA, 8–10 May 2005; IEEE: Piscataway, NJ, USA, 2005.
7. Miao, X.; Chen, X. Natural disasters prevention of power communications system. In Proceedings of the 2010 International Conference on Power System Technology, Hangzhou, China, 24–28 October 2010; IEEE: Piscataway, NJ, USA, 2010.
8. Kwasinski, A.; Weaver, W.; Chapman, P.; Krein, P. Telecommunications power plant damage assessment caused by hurricane katrina—Site survey and follow-up results. In Proceedings of the 2006 International Telecommunications Energy Conference, Piscataway, RI, USA, 10 September 2006; IEEE: Piscataway, RI, USA, 2006.
9. Qiu, L.J. The power grid backbone in the flood—the sideline of flood prevention and protection of the State Grid Zhangzhou Power Supply Company in 2015. *Jiangxi Electr. Power.* **2015**, *39*, 16–17.
10. Liu, X. Seven days and seven nights—Hebei Lishui power supply company to resist the “7·21” catastrophic power grid repair documentary. *State Grid.* **2012**, *9*, 52–54.
11. Guo, Z. Analysis of the impact of flood disasters on the power grid. *China's Strate. Emerg. Ind.* **2018**, *8*, 75.
12. Wang, Y.; Wang, J. Research on hazard damage characteristics and hazard prevention technology of distribution network flood geological hazards. *Power Supply Consum.* **2016**, *33*, 12–18.
13. Hu, B. Look at the damage of flood to transmission and transformation lines and power supply equipment. *Electromech. Int. Mark.* **1999**, *7*, 22–23.

14. Bruno, C.; Canale, S.; Pirri, F. X-SAR SpotLight images feature selection and water segmentation. In Proceedings of the 2012 IEEE International Conference on Imaging Systems and Techniques, Manchester, UK, 16–17 July 2012.
15. Juval, C.; Riihimäki, H.; Pulliainen, J.; Lemmetyinen, J.; Heilimo, J. Implications of boreal forest stand characteristics for X-band SAR flood mapping accuracy. *Remote Sens. Environ.* **2016**, *186*, 47–63.
16. Giustarini, L.; Hostache, R.; Matgen, P.; Bates, P.D.; Mason, D.C.; Schumann, G.J.-P. A change detection approach to flood mapping in urban areas using TerraSAR-X. *IEEE Trans. Geosci. Remote Sens.* **2013**, *51*, 2417–2430. [[CrossRef](#)]
17. Liu, J.; Xu, Z.; Chen, F.; Chen, F.; Zhang, L. Flood hazard mapping and assessment on the Angkor world heritage site, Cambodia. *Remote Sens.* **2019**, *11*, 98. [[CrossRef](#)]
18. Chaabani, C.; Chini, M.; Abdelfattah, R.; Hostache, R.; Chokmani, K. Flood mapping in a complex environment using Bistatic TanDEM-X/TerraSAR-X InSAR coherence. *Remote Sens.* **2018**, *10*, 1873. [[CrossRef](#)]
19. Martinis, S.; Twele, A.; Strobl, C.; Kersten, J.; Stein, E. A Multi-Scale flood monitoring system based on fully automatic MODIS and TerraSAR-X processing chains. *Remote Sens.* **2013**, *5*, 5598–5619. [[CrossRef](#)]
20. Boni, G.; Ferraris, L.; Pulvirenti, L.; Squicciarino, G.; Pierdicca, N.; Candela, L.; Pisani, A.R.; Zoffoli, S.; Onori, R.; Proietti, C.; et al. A prototype system for flood monitoring based on flood forecast combined with COSMO-SkyMed and Sentinel-1 data. *IEEE J. Sel. Top. Appl. Earth Obs. Remote Sens.* **2016**, *9*, 2794–2805. [[CrossRef](#)]
21. Guy, S.; Renaud, H.; Christian, P.; Lucien, H.; Patrick, M.; Florian, P.; Laurent, P. High-Resolution 3-D flood information from radar imagery for flood hazard management. *IEEE Trans. Geosci. Remote Sens.* **2007**, *45*, 1715–1725.
22. Pulvirenti, L.; Pierdicca, N.; Chini, M.; Guerriero, L. Monitoring flood evolution in vegetated areas using COSMO-SkyMed data: The Tuscany 2009 case study. *IEEE J. Sel. Top. Appl. Earth Obs. Remote Sens.* **2013**, *6*, 1807–1816. [[CrossRef](#)]
23. Amitrano, D.; Di Martino, G.; Iodice, A.; Riccio, D.; Ruello, G. Unsupervised rapid flood mapping using Sentinel-1 GRD SAR images. *IEEE Trans. Geosci. Remote Sens.* **2018**, *56*, 3290–3299. [[CrossRef](#)]
24. Deng, J.; Wang, K.; Deng, Y.; Huang, J. An effective way for automatically extracting water body information from SPOT-5 images. *J. Shanghai Jiaotong Univ. Agric. Sci.* **2005**, *2*, 198–201.
25. Chen, L.; Liu, Z.; Zhang, H. SAR image water extraction based on scattering characteristics. *Remote Sens. Technol. Appl.* **2014**, *29*, 963–969.
26. Zeng, L.; Li, L.; Wan, L. SAR-based fast flood mapping using Sentinel-1 imagery. *Geomat. World.* **2015**, *22*, 100–107.
27. Zhang, H.; Fang, W.; Xun, S.; Yang, Y. Flood identification method based on MODIS and GIS and information extraction of land use of submerged area. *J. Catastrophology.* **2010**, *25*, 22–26.
28. Wang, J.; Liu, T.; Yu, Z.; Hu, T.; Zhang, D.; Xun, D.; Wang, D. A research on town flood information rapid extraction based on COSMO-SkyMed and SPOT-5. *Remote Sens. Technol. Appl.* **2016**, *31*, 564–571.
29. Lang, F. *Research on Polarimetric SAR Imagery Filtering and Segmentation*; Wuhan University: Wuhan, China, 2014.
30. Chen, Z. *Flooded Area Classification by High-Resolution SAR Images*; Wuhan University: Wuhan, China, 2017.
31. An, C.; Niu, Z.; Li, Z.; Chen, Z. Otsu threshold comparison and SAR water segmentation result analysis. *J. Electron. Inf. Technol.* **2010**, *32*, 2215–2219. [[CrossRef](#)]
32. An, C.; Cheng, Z. SAR water segmentation based on Otsu and improved CV model. *Signal Process.* **2011**, *2*, 221–225.
33. Lu, J.; Liu, Y.; Wu, C.; Zhang, H.; Zhou, T. Study on satellite monitoring and alarm calculation algorithm of wild fire near transmission lines. *Proc. CSEE* **2015**, *35*, 5511–5519.
34. Lu, J.; Wu, C.; Yang, L.; Zhang, H.; Liu, Y.; Xu, X.J. Research and application of forest fire monitor and early-warning system for transmission line. *Power Syst. Prot. Control* **2014**, *42*, 89–95.
35. Cheng, G.; Han, J.; Lu, X. Remote sensing image scene classification: Benchmark and state of the art. *Proc. CSEE* **2017**, *105*, 1865–1883. [[CrossRef](#)]
36. Jiao, Y.; Wang, S.; Zhou, Y.; Wang, L. Uncertainty analysis of flood disaster assessment using radar imagery. In Proceedings of the 2007 IEEE International Geoscience & Remote Sensing Symposium 2007, Barcelona, Spain, 23–27 July 2007; pp. 4729–4732.

37. Arunangshu, C.; Debasish, C. Computerized seed and range selection method for flood extent extraction in SAR image using iterative region growing. *J. Indian Soc. Remote Sens.* **2019**, *47*, 563–571.
38. D'Addabbo, A.; Refice, A.; Pasquariello, G.; Lovergine, F.P.; Capolongo, D.; Manfreda, S. A bayesian network for flood detection combining SAR imagery and ancillary data. *IEEE Trans. Geosci. Remote Sens.* **2016**, *54*, 3612–3625. [[CrossRef](#)]
39. Pulvirenti, L.; Chini, M.; Pierdicca, N.; Boni, G. Use of SAR data for detecting floodwater in urban and agricultural areas: The Role of the Interferometric Coherence. *IEEE Trans. Geosci. Remote Sens.* **2016**, *54*, 1532–1544. [[CrossRef](#)]
40. Biswajeet, P.; Mahyat, S.T.; Mustafa, N.J. A new semiautomated detection mapping of flood extent from TerraSAR-X satellite image using rule-based classification and taguchi optimization techniques. *IEEE Trans. Geosci. Remote Sens.* **2016**, *54*, 4331–4342.
41. Matgen, P.; Hostache, R.; Schumann, G.; Pfister, L.; Hoffmann, L.; Savenije, H.H.G. Towards an automated SAR based flood monitoring system: Lessons learned from two case studies. *Phys. Chem. Earth Parts A/B/C* **2011**, *36*, 241–252. [[CrossRef](#)]
42. Pulvirenti, L.; Pierdicca, N.; Chini, M.; Guerriero, L. An algorithm for operational flood mapping from synthetic aperture radar (SAR) data based on the fuzzy logic. *Nat. Hazards Earth Syst. Sci.* **2011**, *11*, 529–540. [[CrossRef](#)]
43. Chini, M.; Hostache, R.; Giustarini, L.; Matgen, P. A hierarchical split-based approach for parametric thresholding of SAR images: Flood inundation as a test case. *IEEE Trans. Geosci. Remote Sens.* **2017**, *55*, 6975–6988. [[CrossRef](#)]
44. Hu, Z.; Li, X.; Sun, Y.; Gong, Z.; Wang, Y.; Zhu, L. Flood disaster response and decision-making support system based on remote sensing and GIS. In Proceedings of the 2007 IEEE International Geoscience & Remote Sensing Symposium, Barcelona, Spain, 23–28 July 2007; pp. 2435–2438.
45. Bayraktar, H.; Bayram, B. Fuzzy logic analysis of flood disaster monitoring and assessment of damage in SE Anatolia Turkey. In Proceedings of the 2009 International Conference on Recent Advances in Space Technologies, Istanbul, Turkey, 11–13 June 2009; pp. 13–17.
46. Chen, Y. The comprehensive ranking evaluation of flood disaster based on grey-cloud whitening-weight function. In Proceedings of the 2011 International Conference on Electronic & Mechanical Engineering & Information Technology IEEE, Harbin, China, 12–14 August 2011; pp. 1932–1934.
47. Zhang, Z.; Li, C. Analysis on decision-making model of plan evaluation based on grey relation projection and combination weight algorithm. *J. Syst. Eng. Electron.* **2018**, *4*, 789–796.
48. Krejčí, J.; Petri, D.; Fedrizzi, M. From measurement to decision with the analytic hierarchy process: Propagation of uncertainty to decision outcome. *IEEE Trans. Instrum. Meas. Year.* **2017**, *66*, 3228–3236. [[CrossRef](#)]
49. Kang, H.G.; Seong, P.H. A methodology for evaluating alarm-processing systems using informational entropy-based measure and the analytic hierarchy process. *IEEE Trans. Nucl. Sci.* **1999**, *46*, 2269–2280. [[CrossRef](#)]
50. Bauer-Marschallinger, B.; Paulik, C.; Hochstöger, S.; Mistelbauer, T.; Modanesi, S.; Ciabatta, L.; Massari, C.; Brocca, L.; Wagner, W. Soil moisture from fusion of scatterometer and SAR: Closing the Scale Gap with Temporal Filtering. *Remote Sens.* **2018**, *10*, 1030. [[CrossRef](#)]
51. Chai, X.; Zhang, T.; Shao, Y.; Gong, H.; Liu, L.; Xie, K. Modeling and mapping soil moisture of plateau pasture using RADARSAT-2 imagery. *Remote Sens.* **2015**, *7*, 1279–1299. [[CrossRef](#)]

